Boron Nitride Porous Microbe Its for Hydrogen Storage

ARTICLE *in* ACS NANO · JANUARY 2013

Impact Factor: 12.88 · DOI: 10.1021/nn305320v · Source: PubMed

5 AUTHORS, INCLUDING:

Qunhong Weng
National Institute for Materials Science
21 PUBLICATIONS **263** CITATIONS
SEE PROFILE

Xue-Bin Wang
National Institute for Materials Science
40 PUBLICATIONS **1,036** CITATIONS
SEE PROFILE

Dmitri Golberg
National Institute for Materials Science
643 PUBLICATIONS **22,607** CITATIONS
SEE PROFILE

Boron Nitride Porous Microbelts for Hydrogen Storage

Qunhong Weng,[†,‡,*] Xuebin Wang,[†] Chunyi Zhi,[§,*] Yoshio Bando,[†] and Dmitri Golberg[†,‡,*]

[†]World Premier International Center for Materials Nanoarchitectonics (WPI-MANA), National Institute for Materials Science (NIMS), Namiki 1-1, Tsukuba, Ibaraki 305-0044, Japan, [‡]Graduate School of Pure and Applied Sciences, University of Tsukuba, Tennodai 1, Tsukuba, Ibaraki 305-0005, Japan, and [§]Department of Physics and Materials Science, City University of Hong Kong, Tat Chee Avenue, Kowloon, Hong Kong

ABSTRACT Layered boron nitrides (BNs) are usually viewed as excellent protective coatings and reinforcing materials due to their chemical inertness and high mechanical strength. However, the attention paid to their potential applications in gas sorption, especially in case of hydrogen, has obviously been insufficient. Herein, a novel BN material (*i.e.*, porous microbelts), with the highest specific surface area ever reported for any BN system, up to 1488 $m^2 g^{-1}$, is obtained through one-step template-free reaction of a boron acid—melamine precursor with ammonia. Comprehensive high-resolution transmission electron microscopy, X-ray diffraction, and Raman characterizations all confirm that the obtained BN phase is partially disordered, shows an enlarged average spacing between adjacent (0002) layers (d_{0002} = 0.38 nm, compared to normal 0.33 nm for a bulk layered BN), and belongs to an intermediate state between hexagonal (*h*-BN) and amorphous (*a*-BN) phases. By changing the synthesis temperatures, the textures of obtained porous microbelts are adjustable. H_2 sorption evaluations demonstrate that the materials exhibit high and reversible H_2 uptake from 1.6 to 2.3 wt % at 77 K and at a relatively low pressure of 1 MPa.

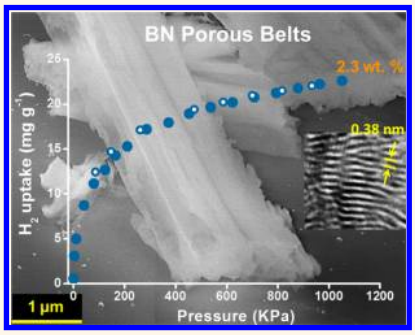

KEYWORDS: boron nitride · porous · microbelts · specific surface area · hydrogen storage

Nanotubes (NTs) and nanosheets (NSs) are two representative low-dimensional nanomorphologies. Both carbon (C) and boron nitride (BN) phases can exist in such forms. Low-dimensional BN nanomaterials are well-known for their excellent chemical inertness and thermal stabilities.[1,2] They provide excellent mechanical reinforcements and enhancement of thermal conductivity in diverse materials, such as polymers, ceramics, and metals.[3−5] In the case of electrically insulating substances, low-dimensional BN nanophases are the better choice than their C counterparts due to their wide energy band gaps (~5−6 eV).[6,7] As a hydrogen adsorbent, both experimental and theoretical studies have demonstrated that BN exhibits a higher H_2 uptake capacity due to its stronger interactions with the heteropolar B−N bonds and partial H_2 chemisorption.[8−11] For example, multiwalled (MW) BNNTs with different morphologies can irreversibly adsorb 0.9−4.2 wt % of H_2 at 10 MPa at room temperature,[8,12] far better than MWCNTs (<1 wt %) at the same testing conditions.[13] However, ~50−70% of the absorbed H_2 was found to be retained when H_2 pressure had been removed.

The dominating H_2 adsorbing mechanism on C and BN surfaces at a low pressure range is physisorption, which is believed to be greatly affected by the specific surface area (SSA) and pore width of an adsorbent.[14] For typical MWBNNTs with an average external diameter of ~50 nm, the reported SSA was 254 $m^2 g^{-1}$ with an estimated pore size, *i.e.*, tube inner diameter of ~20 nm.[8] In order to obtain porous BN with an increased SSA and reduced pore size, the hard-template-based synthesis was the commonly adopted strategy. For example, when silica was used as a template, the reported SSAs of obtained BNs were 140−327 $m^2 g^{-1}$.[15−17] Mesoporous BN materials with the SSAs ranging from 168 to 565 $m^2 g^{-1}$ and having ~3 nm pores were prepared by using activated carbon as the template.[15,18,19] Further increase of SSAs in mesoporous BN materials was achieved when some other templates, such as cationic surfactant (820 $m^2 g^{-1}$) and zeolite (570 $m^2 g^{-1}$), had been utilized.[20,21] However, the SSAs and pore widths of these template-derived porous BN materials were still not satisfactory for commercial hydrogen storage. Besides,

* Address correspondence to weng.qunhong@nims.go.jp, cy.zhi@cityu.edu.hk, golberg.dmitri@nims.go.jp.

Received for review November 16, 2012 and accepted January 9, 2013.

Published online January 09, 2013
10.1021/nn305320v

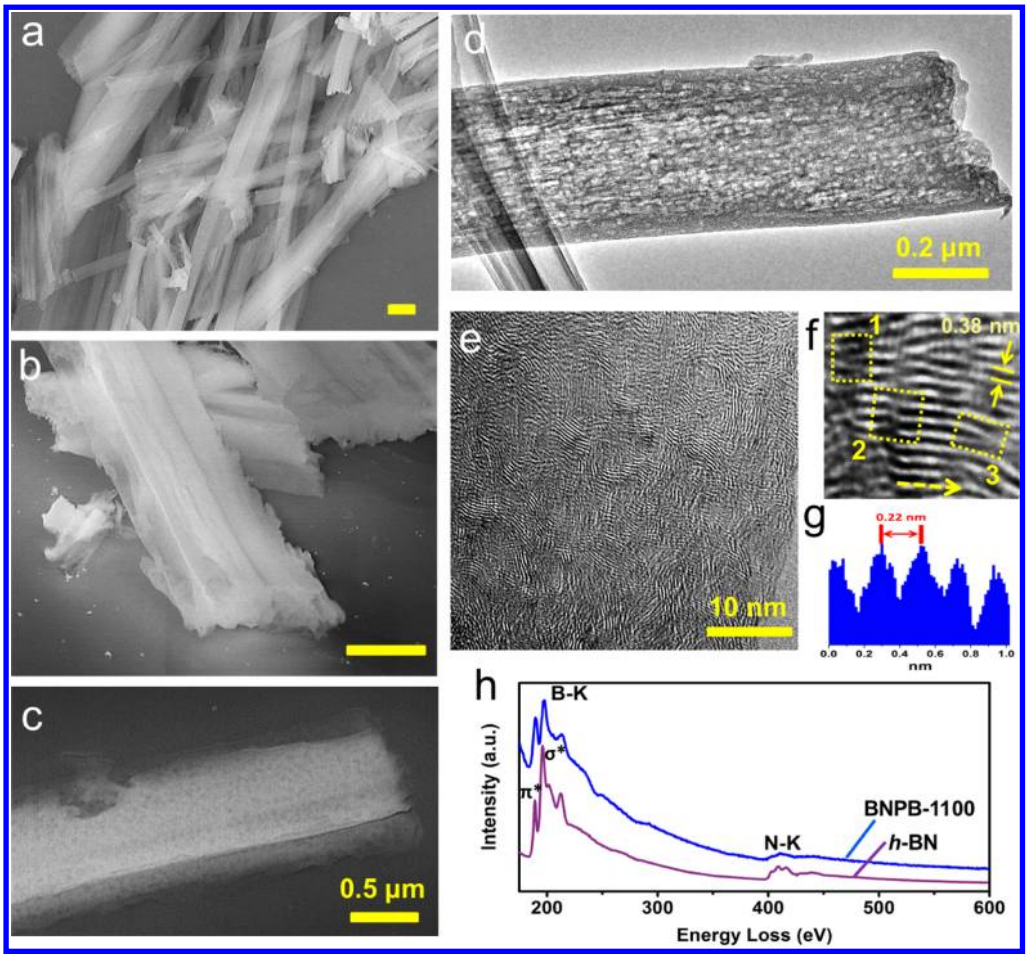

Figure 1. (a) Low-magnification SEM image of BN porous microbelts obtained at 1100 °C (BNPB-1100). (b,c) Tilted and top views of isolated porous structures, revealing a clear belt-shaped morphology. (d) TEM image of a belt section at a low magnification. (e,f) HRTEM images taken at the belt edge. Three typical dislocation structures are labeled by yellow dashed frames. (g) TEM contrast intensity profile recorded along the yellow dashed arrow marked in (f). (h) EELS profile taken from a typical BN porous microbelt. The EEL spectrum of *h*-BN is also shown for comparison. Scale bars in (a) and (b) are 1 μm.

this method also suffers from other drawbacks, such as inefficient filling of the mesopores by precursors and harmful reagents needed for template removal. Thus, there is an increased demand for development of nontemplate methods and design of user-friendly porous BN hydrogen accumulators. It would also be important to clarify the relationship between the BN material morphology/texture and its hydrogen uptake once the simpler methods become available for the porous BN material synthesis. To the best of our knowledge, the few-layered *h*-BN sheets prepared from boric acid and urea have indeed been reported, and those exhibit the highest SSA among all non-template-derived BNs (927 $m^2\ g^{-1}$).[22]

In the present study, we develop an easily operable method for preparing novel BN porous microbelts with the highest reported SSAs ranging from 1144 to 1488 $m^2\ g^{-1}$. The synthesis process was completed *via* a one-step, ambient pressure, template-free reaction between boric acid–melamine (2B·M) precursors and ammonia at 900–1100 °C corresponding to BNPB-900, BNPB-1000, and BNPB-1100 sample notations used throughout the paper. The sample morphology and elemental compositions were comprehensively characterized by using scanning electron microscopy (SEM), X-ray diffraction (XRD), energy-dispersive X-ray spectroscopy (EDS), high-resolution transmission electron microscopy (HRTEM), and electron energy loss spectroscopy (EELS). N_2 physisorption isotherms recorded at 77 K were used to calculate the material pore size distributions and SSAs based on the Brunauer–Emmett–Teller (BET) equation, while H_2 uptake was measured by analyzing H_2 isotherms recorded at 77 K and at a relatively low pressure of 1 MPa. It was demonstrated that the present high-surface-area BN porous microbelts exhibit decent and reversible hydrogen uptake, from 1.6 to 2.3 wt %. Among all samples, BNPB-1100 had the highest hydrogen uptake capacity.

RESULTS AND DISCUSSION

The BNPB-1100 shows a belt-like structure, a typical BN morphology derived from 2B·M precursors at a high temperature. The SEM images verify that the belt width and thickness are commonly in the range of

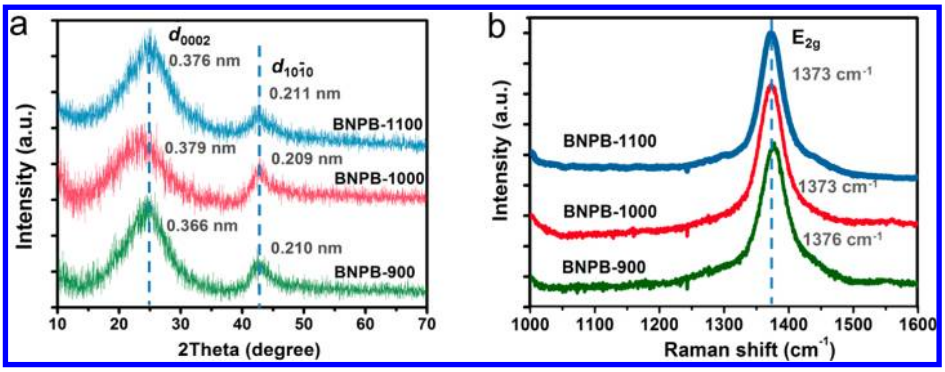

Figure 2. XRD patterns (a) and Raman spectra (b) of BN porous microbelts prepared at different temperatures (BNPB-900, BNPB-1000, and BNPB-1100).

0.3−1.0 and 0.2−0.5 μm, respectively, with the length varying from ∼10 μm to hundreds of micrometers (Figure 1a). Ultrashort and ultralong belts were also occasionally found. Unlike the smooth appearances of multiwalled CNT and BNNT surfaces, many sheet-like portions protrude from the belts and structural voids/breakages are easily observed on their surfaces (Figure 1b). Fine structural SEM and TEM analyses further indicate that there are many pores randomly distributed on the belt surfaces, leading to an overall featured perforated appearance (Figure 1c,d). A high porosity of the structures is indeed apparent. HRTEM characterizations (Figure 1f) on many belt edges reveal that the average spacing between adjacent (0002) fringes is 0.38 nm, far larger than the (0002) interplanar distance in bulk *h*-BN and MWBNNTs (0.33−0.34 nm).[23] Such enlarged spacing was further confirmed by X-ray diffraction (XRD) patterns which revealed a deduced lattice parameter d_{0002} = 0.376 nm based on the corresponding (0002) peak position, as shown in Figure 2a. The obtained in-plane lattice spacing is 0.21 nm; this is in close accordance with the HRTEM observations (∼0.22 nm, Figure 1f,g). It is noteworthy that the ordering type observed for this novel porous BN material is an intermediate between classical hexagonal (*h*-BN) and amorphous (*a*-BN) phases and seems to be closer to that in the well-known turbostratic BN materials (*t*-BN, d_{0002} = 0.356 nm).[24−26] It is noted that dislocation structures are common in the present BN phases. Three representative dislocation structures, radical-rich edge dislocation (1), helical screw dislocations (2), and Y-form dislocations (3), are shown in Figure 1f. These dislocation types are similar to the observations in anthracites reported recently.[27] Other BN porous microbelt samples that were obtained at different temperatures also showed similar structural features (see Figure S2, Supporting Information).

Both amorphous-like and crystalline phases (Figure 1e) coexist in the product. The most characteristic change in XRD patterns caused by a partial disorder of BN phase is seen as broadened and less intense (0002) and (10$\bar{1}$0) peaks at 2θ = 23.22−24.31 and 42.89−43.13°, respectively. With an increase in the synthesis temperature, the (0002) patterns of the products slightly downshift as the derived d_{0002} values increase from 0.366 nm (BNPB-900) to ∼0.38 nm (BNPB-1000 and BNPB-1100). See Figure 2a.

The Raman shift and fwhm of the E_{2g} vibration were commonly used to evaluate the crystalline structure and ordering of hexagonal and other layered BN structures. It is well-known that high-quality *h*-BN single crystals show an intrinsic E_{2g} vibration peak at 1367 cm^{-1} with the fwhm of 9.1 cm^{-1}.[28] For polycrystalline BN, its E_{2g} mode is shifting to a higher frequency from 1367 to 1374 cm^{-1}, as the crystal domain size decreases, with the fwhm increasing from 11 to 42 cm^{-1}, respectively.[29] Raman shift and fwhm are also sensitive to the number of layers in *h*-BN. With a decrease in this number, to a monolayer, the E_{2g} mode shifts to a higher frequency (∼1369 cm^{-1}) with a slight increase of fwhm to 10−12 cm^{-1}.[30] Figure 2b shows the sharp E_{2g} peaks at 1376, 1373, and 1373 cm^{-1} of the as-prepared BN porous microbelts obtained at 900, 1000, and 1100 °C; these have fwhm values of ∼56, 43, and 38 cm^{-1}, respectively. An upshift of E_{2g} vibration mode to the higher frequency compared to the bulk *h*-BN indicates a weaker interaction between interlayers in BN porous microbelts, whereas the obvious broadening of the E_{2g} peak reflects clear size shrinking of the ordered BN phase. Further annealing of the BNPB-1100 sample at 1500 °C for 5 h could not remarkably improve its ordering. In Figure S3 of the Supporting Information, the resultant d_{0002} is seen to decrease from 0.376 to 0.364 nm after annealing, while the resultant E_{2g} vibration mode in Raman spectra (Figure S3b) shifts to 1370 cm^{-1} without obvious change of the fwhm value. The observed dislocation structures that exist in the present BN porous microbelts provide a reasonable explanation for such high thermal stability. They not only widen the average BN (0002) layer distances but also "screw" neighboring layers together, and thus provide considerable strength to avoid further ordering of BN (0002) layers at a high temperature (*e.g.*, 1500 °C, similar to

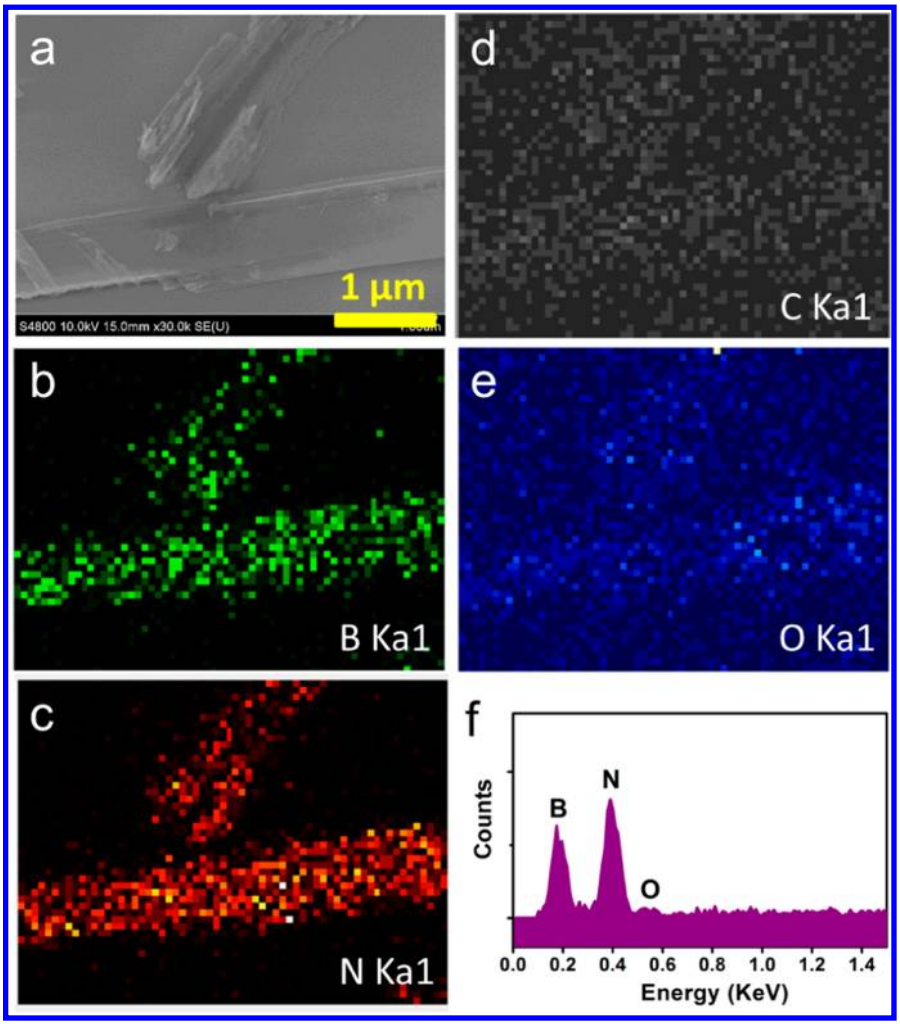

Figure 3. SEM image (a) and corresponding B, N, C, and O maps (b−e) of BNPB-1100. (f) Accumulated energy-dispersive X-ray spectrum (EDS), confirming decently pure BN composition.

providing strength to suppress the solubility in case of anthracite[27]).

The chemical composition of the samples was verified by EELS and EDS. An EEL spectrum of BNPB-1100 reveals distinct B and N core loss K-edges at 188 and 401 eV, respectively, as shown in Figure 1h. A trace of the C K-edge at 284 eV is also detected. The π^* and σ^* peak shapes on the left- and right-hand sides of B and N K-edges are not as sharp as in a standard *h*-BN, also suggesting that the as-prepared BN porous belts belong to an intermediate state between *a*-BN and *h*-BN.[31] This observation is in accordance with our discussions for the HRTEM, XRD, and Raman result sections. Figure 3a depicts a typical morphology of the BNPB-1100 sample. Figure 3b,c shows corresponding spatially resolved B and N maps. Figure 3d is a C map, in which C signals are randomly distributed over the whole investigated area. The accumulated EDS spectrum measured over the sample area of 0.01 mm^2 is displayed in Figure 3f, suggesting that the sample mainly consists of B and N with a trace amount of oxygen. A quantitative analysis based on the EDS results gave a (B + N) sum of 97 atom %. The EDS spectra of BNPB-900 and BNPB-1000 samples are shown in Figure S4, Supporting Information. These also confirm decently pure BN compositions. It should be noted that the oxygen content within the samples increased quickly if the synthesis temperatures were lower than 900 °C; for example, the oxygen content could reach ~6 atom % for a porous microbelt sample synthesized at 700 °C.

Compared with organic ammonia borane or borazine precursors, the advantage of using 2B·M precursors is the ease in their production and their low cost. However, in addition to providing N source, melamine also contains C atoms. The key challenge for the utilization of 2B·M precursors is to eliminate C atoms in the resultant products.[32] Before this report, a lot of BN nanomaterials, including BNNTs, nanofibers, nanocable coatings, *etc.*, have been prepared based on the 2B·M precursors.[33−35] In order to avoid C contamination, an extra high temperature was usually implemented to obtain pure BN compositions; for example, heating in an induction furnace was carried out at

1700−2000 °C.[33,36] At such high temperature, it was difficult to maintain the original BN nanomorphology, and this unavoidably led to the recrystallization of a BN phase. By contrast, our results provide a facile route to fabricate highly pure BN materials during the reaction of 2B·M precursors with ammonia at the ambient pressure and a relatively low temperature, $P = 1$ atm, $T \geq 900$ °C. The product yield was as high as 20 wt % with respect to the raw 2B·M precursor and can be easily scaled up. The product morphology is controllable because the appearance of precursors can be diversified by different crystallization conditions. Besides O_2, it is also known that carbonaceous composition can be removed from BN *via* the reaction with ammonia at 1000 °C along with the following reaction:[21]

$$C + NH_3 \rightarrow CH_4 + N_2 \quad (1)$$

Experimentally, providing excess ammonia would favor the complete conversion of B_2O_3 to BN and offset the loss of ammonia due to the decomposition of melamine.

To determine the BET SSA of the samples, we measured their N_2 adsorption and desorption isotherms at 77 K. For mesoporous and macroporous materials, the standard BET analysis is performed at a pressure range of $0.05 < P/P_0 < 0.35$.[37] In general, without micropores or any other type of strongly adsorbing sites, this range can be linearly fitted. However, for microporous materials, this selection criterion is no longer applicable because all pores would be completely filled with N_2 molecules at pressures below the standard BET range. Thus, the respective pressure range chosen for the multipoint BET analysis of the present microporous BN samples was from 0.02 to 0.12 based on the criteria proposed elsewhere.[38] For the detailed selection procedure, see Supporting Information. The resultant BET SSAs were 1161, 1488, and 1144 $m^2\ g^{-1}$ for BNPB-900, BNPB-1000, and BNPB-1100, respectively, and these figures are the largest SSAs reported to date for any BN material system.

The isotherms and hysteresis loops of all BN porous microbelt samples obtained at different temperatures belong to the typical type I isotherm and type H4 loop (based on the IUPAC classification), indicating microporosity and containing slit-shaped mesopores that are associated with capillary condensation. Nonlocal density functional theory[39] (NLDFT) was implemented to calculate the pore widths and pore size distributions for the samples. As illustrated in Figure 4b and Table S2, all BN porous microbelt samples display high microporosity (0.350−0.502 $cm^3\ g^{-1}$) as well as meso- and macroporosities (0.348−0.530 $cm^3\ g^{-1}$) with an average micropore width of 1.1 nm. The total pore volume determined at $P/P_0 = 0.99$ reaches 0.880 $cm^3\ g^{-1}$ for BNPB-1100. Although the total pore volumes increase with an increase of the synthesis temperature, the BNPB-1000 sample has the largest micropore volume

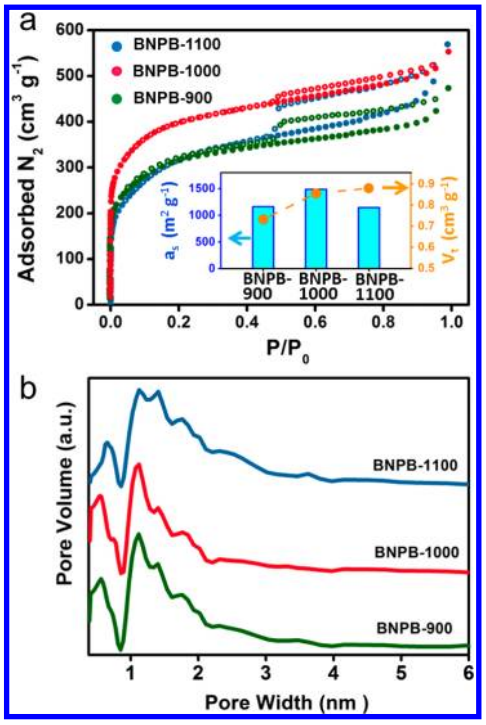

Figure 4. (a) Nitrogen adsorption−desorption isotherms of BN porous microbelts prepared at different temperatures (BNPB-900, BNPB-1000, and BNPB-1100). The inset in (a) is the summary of BET surface areas (a_s) and total pore volumes (V_t) measurements for the obtained samples. (b) Pore size distribution profiles of microbelts derived by using nonlocal density functional theory.

of 0.502 $cm^3\ g^{-1}$. Such high microporosity and SSAs of these novel BN porous microbelts may also result from the dislocation structures that are discussed above. The number of slit-shaped pores with a large enough width to adsorb N_2 molecules increases simultaneously with the expansion of average BN (0002) layer distances (their pore widths obey statistical distributions, as predicted by the interlayer distance statistics and XRD patterns). As a result, the micropore volume and SSA values that can be probed by the N_2 adsorption−desorption method for these BN porous materials increase accordingly.

The H_2 adsorption and desorption isotherms of BN porous belts, measured by the volumetric method at 77 K and 1 MPa, are shown in Figure 5. With an increase in the synthesis temperature from 900 to 1100 °C, the samples exhibit enhanced H_2 uptake, from 1.6 to 2.3 wt %, which obviously do not follow their textural properties, such as SSAs or micropore volumes. BNPB-1100 shows the highest H_2 uptake of 2.3 wt %. For comparison, the H_2 uptake of bulk *h*-BN measured at the same conditions shows a negligible adsorption, much less than 0.1 wt %. However, further increase of the synthesis temperature was not able to improve the H_2 uptake. Although all sorption isotherms are fully reversible, the larger steady slope of BNPB-1100 indicates that, compared to other samples, even higher H_2 uptake can be expected at a higher pressure.

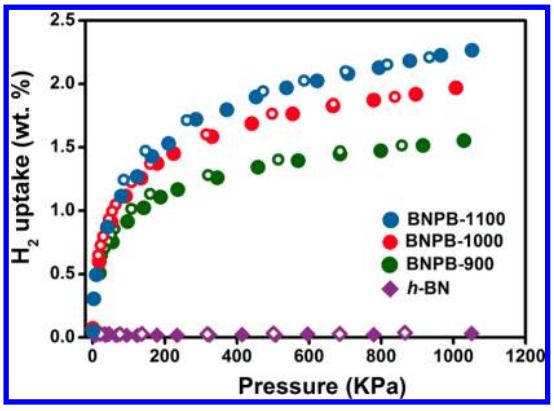

Figure 5. Hydrogen adsorption–desorption isotherms at 77 K and 1 MPa of BN porous microbelts. For comparison, the hydrogen uptake of bulk *h*-BN is also shown.

Hydrogen can be stored or retained along with chemisorption or physisorption mechanisms. H_2 uptake in metal hydrides and organic BN compounds is typically based on chemisorption, while H_2 adsorptions in metal–organic frameworks (MOFs), porous carbons, and polymers belong to the physorption category.[13] The threshold condition (estimated by U.S. Department of Energy) for application as an economically feasible hydrogen storage material requires 6.5 wt % uptake of H_2 at 2 MPa and room temperature.[40] Usually, for chemisorption-based materials, reaching this absolute uptake value is not difficult. The main challenge is how to satisfy the required low pressure and room temperature conditions simultaneously. On the contrary, the used H_2 pressures in physorption-based materials are much lower, typically from 0.1 MPa to several MPa. Their H_2 uptake and storage temperature (usually 77 K) become a concern instead. As a representative storage material that relies on physisorption, more and more proof predicts that H_2 uptake capacities in microporous carbons are proportional to their SSAs and micropore volumes.[41,42] However, this conclusion is not totally applicable to pure BN or BCN systems.[43] Such peculiar H_2 adsorption behavior may be caused by the intrinsic heterogeneous adsorption property of H_2 molecules on BN surfaces. Some H_2 adsorbing sites with higher H_2 affinity are more "active" to adsorb H_2 molecules. Further clarifying of these active adsorbing sites and synthesis of porous BN materials with controlled densities of such sites would be definitely helpful to find more effective and commercially applicable H_2 storage materials based on a nano- and/or micro-BN system.

SUMMARY

In summary, the present study enlightens a simple route to prepare highly porous BN materials (*i.e.*, BN porous microbelts) using a one-step, template-free reaction of a boron acid–melamine precursor with ammonia under moderate conditions. The obtained porous belts are partially disordered and show an enlarged spacing between adjacent (0002) layers, thus belonging to an intermediate state between hexagonal and amorphous BN phases. The sample prepared at 1000 °C shows the largest SSA and micropore volume, reaching 1488 $m^2\ g^{-1}$ (*i.e.*, the highest value ever reported for any BN material) and 0.502 $cm^3\ g^{-1}$, respectively, whereas the 1100 °C-derived BN porous belt sample exhibits the largest total pore volume of 0.880 $cm^3\ g^{-1}$. H_2 uptake measurements performed at 77 K and 1 MPa in fact confirm that the latter sample possesses the largest reversible H_2 uptake capacity of 2.3 wt %.

METHODS

Synthesis of BN Porous Microbelts. First, 0.03 mol boric acid and 0.015 mol melanine (2B·M) were dissolved in ~70 mL of 90 °C deionized (DI) water. The solution was then heated and kept at a slightly boiling state to completely evaporate of the water, thus 2B·M adducts were obtained. Then, the dried 2B·M precursors were loaded into a horizontal quartz tube and heated in an ammonia atmosphere at preset temperatures for 3 h, yielding the mixture of BN microrods (bundles composed of aligned porous microbelts, Figure S1, Supporting Information) and BN porous microbelts. The received mixtures containing BN microrods were dispersed in isopropyl alcohol and exfoliated by supersonication for 30 min to obtain isolated belts and loosened belt bundles. Prolonged sonication time increases the content of the isolated belts.

Structure and Composition Characterization. The morphology and structure observations were carried out by using a Hitachi S-4800 SEM and JEM-3000F HRTEM operated at 300 kV. Chemical compositions were determined by an EMAX EDS and Gatan 766 EELS 2D-DigiPEELS. XRD data were collected on a Rigaku Ultima III (Cu Kα); Raman data were recorded on a Horiba Jobin-Yvon T6400 Raman system with a 514.5 nm excitation laser. The laser intensity exposed to the samples was estimated to be around 10 mW (50× optical lens) with an accumulation time of 20 s for each spectrum.

Specific Surface Area Measurements and H_2 Uptake Capacity Evaluations. The nitrogen physisorption isotherms were recorded at 77 K on a Quantachrome Autosorb-1 system after outgassing of samples at 150 °C for 24 h. Specific surface areas were calculated by the Brunauer–Emmett–Teller (BET) equation using the relative pressure range from 0.02 to 0.12 (see Supporting Information for more details). The pore size distribution, combining respective pore volume, and average pore size were calculated based on the NLDFT theory. The hydrogen adsorption and desorption isotherms were taken on a BELSORP-HP-30 hydrogen adsorption system (BEL Japan, Inc.) at 77 K and a 0–1 MPa pressure range. Before the measurements, all samples were outgassed at 150 °C for 24 h.

Conflict of Interest: The authors declare no competing financial interest.

Acknowledgment. The authors thank Drs. M. Nakatsu, K. Iiyama, N. Kawamoto, A. Nukui, and M. Mitome for their generous technical assistance. This work was funded by the World Premier International Center for Materials Nanoarchitectonics (WPI-MANA) of NIMS, Tsukuba, Japan.

Supporting Information Available: Structures of BN microrods, loosened belt bundles, and isolated belts; morphology of BNPB-900 and BNPB-1000 samples; list of Raman shifts for all samples; evolution of XRD, Raman spectra, and HRTEM

of BNPB-1100 after annealing at 1500 °C; chemical compositions of BNPB-900 and BNPB-1000 samples; P/P_0 range selections and seven-point linear simulation of BET equiation; textural characteristics and hydrogen uptake summary table of all products. This material is available free of charge *via* the Internet at http://pubs.acs.org.

REFERENCES AND NOTES

1. Golberg, D.; Bando, Y.; Kurashima, K.; Sato, T. Synthesis and Characterization of Boron Nitride Multiwalled Nanotube Ropes. *Scr. Mater.* **2001**, *44*, 1561–1564.
2. Chen, Y.; Zou, J.; Campbell, S. J.; Caer, G. L. Boron Nitride Nanotubes: Pronounced Resistance to Oxidation. *Appl. Phys. Lett.* **2004**, *84*, 2430–2432.
3. Huang, Q.; Bando, Y.; Xu, X.; Nishimura, T.; Zhi, C. Y.; Tang, C. C.; Xu, F. F.; Gao, L.; Golberg, D. Enhancing Superplasticity of Engineering Ceramics by Introducing BN Nanotubes. *Nanotechnology* **2007**, *18*, 485706.
4. Zhi, C. Y.; Bando, Y.; Tang, C. C.; Kuwahara, H.; Golberg, D. Large-Scale Fabrication of Boron Nitride Nanosheets and Their Utilization in Polymeric Composites with Improved Thermal and Mechanical Properties. *Adv. Mater.* **2009**, *21*, 2889–2893.
5. Wang, X. B; Zhi, C. Y; Li, L.; Zeng, H. B.; Li, C.; Mitome, M.; Golberg, D.; Bando, Y. "Chemical Blowing" of Thin-Walled Bubbles: High-Throughput Fabrication of Large-Area, Few-Layered BN and Cx-BN Nanosheets. *Adv. Mater.* **2011**, *23*, 4072–4076.
6. Zhi, C. Y.; Bando, Y.; Terao, T. S.; Tang, C. C.; Golberg, D. Dielectric and Thermal Properties of Epoxy/Boron Nitride Nanotube Composites. *Pure Appl. Chem.* **2010**, *82*, 2175–2183.
7. Tijerina, J. T.; Narayanan, T. N.; Gao, G.; Rohde, M.; Tsentalovich, D.; Pasquali, M.; Ajayan, P. M. Electrically Insulating Thermal Nano-Oils Using 2D Fillers. *ACS Nano* **2012**, *6*, 1214–1220.
8. Ma, R. Z.; Bando, Y.; Zhu, H. W.; Sato, T.; Xu, C. L.; Wu, D. H. Hydrogen Uptake in Boron Nitride Nanotubes at Room Temperature. *J. Am. Chem. Soc.* **2002**, *124*, 7672–7673.
9. Wang, P.; Orimo, S.; Matsushima, T.; Fujii, H.; Majer, G. Hydrogen in Mechanically Prepared Nanostructured h-BN: A Critical Comparison with That in Nanostructured Graphite. *Appl. Phys. Lett.* **2002**, *80*, 318–320.
10. Jhi, S. H.; Kwon, Y. K. Hydrogen Adsorption on Boron Nitride Nanotubes: A Path to Room-Temperature Hydrogen Storage. *Phys. Rev. B* **2004**, *69*, 245407.
11. Lim, S. H.; Luo, J. Z.; Ji, W.; Lin, J. Synthesis of Boron Nitride Nanotubes and Its Hydrogen Uptake. *Catal. Today* **2007**, *120*, 346–350.
12. Tang, C. C.; Bando, Y.; Ding, X. X.; Qi, S. R.; Golberg, D. Catalyzed Collapse and Enhanced Hydrogen Storage of BN Nanotubes. *J. Am. Chem. Soc.* **2002**, *124*, 14550–14551.
13. Van den Berg, A. W. C.; Otero Arean, C. Materials for Hydrogen Storage: Current Research Trends and Perspectives. *Chem. Commun.* **2008**, 668–681.
14. Yang, S. J.; Kim, T.; Im, J. H.; Kim, Y. S.; Lee, K.; Park, C. R. MOF-Derived Hierarchically Porous Carbon with Exceptional Porosity and Hydrogen Storage Capacity. *Chem. Mater.* **2012**, *24*, 464–470.
15. Dibandjo, P.; Chassagneux, F.; Bois, L.; Sigala, C.; Miele, P. Comparison between SBA-15 Silica and CMK-3 Carbon Nanocasting for Mesoporous Boron Nitride Synthesis. *J. Mater. Chem.* **2005**, *15*, 1917–1923.
16. Rushton, B.; Mokaya, R. Mesoporous Boron Nitride and Boron−Nitride−Carbon Materials from Mesoporous Silica Templates. *J. Mater. Chem.* **2008**, *18*, 235–241.
17. Alauzun, J. G.; Ungureanu, S.; Brun, N.; Bernard, S.; Miele, P.; Backov, R.; Sanchez, C. Novel Monolith-Type Boron Nitride Hierarchical Foams Obtained through Integrative Chemistry. *J. Mater. Chem.* **2011**, *21*, 14025–14030.
18. Han, W. Q.; Brutchey, R.; Tilley, T. D.; Zettl, A. Activated Boron Nitride Derived from Activated Carbon. *Nano Lett.* **2004**, *4*, 173–176.
19. Vinu, A.; Terrones, M.; Golberg, D.; Hishita, S.; Ariga, K.; Mori, T. Synthesis of Mesoporous BN and BCN Exhibiting Large Surface Areas *via* Templating Methods. *Chem. Mater.* **2005**, *17*, 5887–5890.
20. Dibandjo, P.; Bois, L.; Chassagneux, F.; Miele, P. Thermal Stability of Mesoporous Boron Nitride Templated with a Cationic Surfactant. *J. Eur. Ceram. Soc.* **2007**, *27*, 313–317.
21. Schlienger, S.; Alauzun, J.; Michaux, F.; Vidal, L.; Parmentier, J.; Gervais, C.; Babonneau, F.; Bernard, S.; Miele, P.; Parra, J. B. Micro-, Mesoporous Boron Nitride-Based Materials Templated from Zeolites. *Chem. Mater.* **2012**, *24*, 88–96.
22. Nag, A.; Raidongia, K.; Hembram, K. P. S. S.; Datta, R.; Waghmare, U. V.; Rao, C. N. R. Graphene Analogues of BN: Novel Synthesis and Properties. *ACS Nano* **2010**, *4*, 1539–1544.
23. Golberg, D.; Bando, Y.; Huang, Y.; Terao, T.; Mitome, M.; Tang, C. C.; Zhi, C. Y. Boron Nitride Nanotubes and Nanosheets. *ACS Nano* **2010**, *4*, 2979–2993.
24. Thomas, J.; Weston, N. E.; O'Connor, T. E. Turbostratic Boron Nitride, Thermal Transformation to Ordered-Layer-Lattice Boron Nitride. *J. Am. Chem. Soc.* **1962**, *84*, 4619–4622.
25. Hamilton, E. J. M.; Dolan, S. E.; Mann, C. M.; Colijn, H. O.; Shore, S. G. Preparation of Amorphous Boron Nitride from the Reaction of Haloborazines with Alkali Metals and Formation of a Novel Tubular Morphology by Thermal Annealing. *Chem. Mater.* **1995**, *7*, 111–117.
26. Zhao, Z. Y.; Yang, Z. G.; Wen, Y.; Wang, Y. H. Facile Synthesis and Characterization of Hexagonal Boron Nitride Nanoplates by Two-Step Route. *J. Am. Ceram. Soc.* **2011**, *94*, 4496–4501.
27. Sun, Y. Q.; Alemany, L. B.; Billups, W. E.; Lu, J. X.; Yakobson, B. I. Structural Dislocations in Anthracite. *J. Phys. Chem. Lett.* **2011**, *2*, 2521–2524.
28. Kubota, Y.; Watanabe, K.; Tsuda, O.; Taniguchi, T. Deep Ultraviolet Light-Emitting Hexagonal Boron Nitride Synthesized at Atmospheric Pressure. *Science* **2007**, *317*, 932–934.
29. Nemanich, R. J.; Solin, S. A.; Martin, R. M. Light Scattering of Boron Nitride Microcrystals. *Phys. Rev. B* **1981**, *23*, 6348–6356.
30. Gorbachev, R. V.; Riaz, I.; Nair, R. R.; Jalil, R.; Britnell, L.; Belle, B. D.; Hill, E. W.; Novoselov, K. S.; Watanabe, K.; Taniguchi, T.; *et al.* Hunting for Monolayer Boron Nitride: Optical and Raman Signatures. *Small* **2011**, *7*, 465–468.
31. Huang, J. Y.; Yasuda, H.; Mori, H. HRTEM and EELS Studies on the Amorphization of Hexagonal Boron Nitride Induced by Ball Milling. *J. Am. Ceram. Soc.* **2000**, *83*, 403–409.
32. Singh, L.; Chopra, V. Effect of Preparation Conditions on the Crystallinity of Chemically Synthesized BCNO Nanophosphor. *J. Mater. Sci. Technol.* **2011**, *27*, 967–972.
33. Ma, R.; Bando, Y.; Sato, T. CVD Synthesis of Boron Nitride Nanotubes without Metal Catalysts. *Chem. Phys. Lett.* **2001**, *337*, 61–64.
34. Yin, L. W.; Bando, Y.; Golberg, D.; Gloter, A.; Li, M. S.; Yuan, X. L.; Sekiquchi, T. Porous BCN Nanotubular Fibers: Growth and Spatially Resolved Cathodoluminescence. *J. Am. Chem. Soc.* **2005**, *127*, 16354–16355.
35. Zhu, Y. C.; Bando, Y.; Ma, R. Aluminum Borate−Boron Nitride Nanocables. *Adv. Mater.* **2003**, *15*, 1377–1379.
36. Hagio, T.; Kobayashi, K.; Sato, T. Formation of Hexagonal BN by Thermal Decomposition of Melamine Diborate. *J. Ceram. Soc. Jpn.* **1994**, *102*, 1051–1054.
37. Sing, K. S. W.; Everett, D. H.; Haul, R. A. W.; Moscou, L.; Pierotti, R. A.; Rouquerol, J.; Siemieniewska, T. Reporting Physisorption Data for Gas/Solid Systems with Special Reference to the Determination of Surface Area and Porosity. *Pure Appl. Chem.* **1985**, *57*, 603–619.
38. Rouquerol, J.; Llewellyn, P.; Rouquerol, F. Is the BET Equation Applicable to Microporous Adsorbents? *Stud. Surf. Sci. Catal.* **2007**, *160*, 49–56.
39. Evans, R.; Tarazona, P. Theory of Condensation in Narrow Capillaries. *Phys. Rev. Lett.* **1984**, *52*, 557–560.
40. Deng, W. Q.; Xu, X.; Goddard, W. A. New Alkali Doped Pillared Carbon Materials Designed To Achieve Practical Reversible Hydrogen Storage for Transportation. *Phys. Rev. Lett.* **2004**, *92*, 166103.

41. Gogotsi, Y.; Dash, R. K.; Yushin, G.; Yildirim, T.; Laudisio, G.; Fischer, J. E. Tailoring of Nanoscale Porosity in Carbide-Derived Carbons for Hydrogen Storage. *J. Am. Chem. Soc.* **2005**, *127*, 16006–16007.
42. Yushin, G.; Dash, R.; Jagiello, J.; Fischer, J. E.; Gogotsi, Y. Carbide-Derived Carbons: Effect of Pore Size on Hydrogen Uptake and Heat of Adsorption. *Adv. Funct. Mater.* **2006**, *16*, 2288–2293.
43. Portehault, D.; Giordano, C.; Gervais, C.; Senkovska, I.; Kaskel, S.; Sanchez, C.; Antonietti, M. High-Surface-Area Nanoporous Boron Carbon Nitrides for Hydrogen Storage. *Adv. Funct. Mater.* **2010**, *20*, 1827–1833.